Effective radiative cooling in optically thin plasmas

T. Schmutzler^{1,2} and W. M. Tscharnuter²

¹ Max-Planck-Institut für Kernphysik, Saupfercheckweg 1, W-6900 Heidelberg 1, Germany

Received September 4, 1992; accepted February 19, 1993

Abstract. We present the radiative cooling rates and cooling timescales of an optically thin atomic gas for the temperature range 10² K to 10⁹ K, calculated in a thermally self-consistent, time-dependent approach. The most important emission lines of the ten most abundant elements have been considered as well as the relevant continuum processes. We compare the cooling rate of a gas in collisional ionization equilibrium with those of gases with nonequilibrium ionization. We also compare the time-dependent ionization states of all considered elements with those of steady-state calculations. Time-dependent ionization stages, cooling rates and timescales are influenced by the previous history of the gas and by the thermodynamical path (e.g., isochoric or isobaric) of cooling. As basic applications we investigate the rôle of the metallicity and of the interstellar photon field for the effective time-dependent cooling in thin gases.

Key words: atomic processes – interstellar medium: general – plasmas

1. Introduction

Radiative cooling of an optically thin gas leads to a strong deviation from equilibrium ionization and therefore to a different energy-loss rate than in the commonly assumed case of gas radiating in collisional ionization equilibrium (CIE). This is a consequence of the cooling timescale being shorter than the relevant recombination timescales. Although this fact has been known for the temperature range from 10⁴ K to 2 10⁶ K at least since the work of Kafatos (1973) and Shapiro & Moore (1976), it has not been considered generally in studies of thin astrophysical plasmas or for interpretations of observations. Many sophisticated models have been developed, especially in the research field of supernova remnants, including time-dependent ionization rates (e.g., Cox 1972; Dere et al. 1981; Hamilton et al. 1983, 1984; Hughes & Helfand 1985; Innes 1985; Innes et al. 1987a, 1987b, 1987c; Gaetz et al. 1988; Brinkmann et al. 1989;

Send offprint requests to: T. Schmutzler, Institut für Theoretische Astrophysik

Innes 1992). However, we have not found any thermally self-consistent treatment of this complex, highly non-LTE evolution of atomic gases. One reason might be the large amount of computing time which is necessary for self-consistent solutions and the fact that studies using different boundary conditions require totally independent calculations. However, desk-top computers have now become available which could perform such calculations overnight.

From observations of their radiative spectra and from absorption measurements we know that optically thin astrophysical plasmas exist in a wide range of temperatures from several thousand Kelvin up to few billion Kelvin. The interstellar medium of our Galaxy, for instance, contains various states of atomic gas with temperatures differing by factors of hundreds to tens of thousands. Parts of these gas states may exist in a stable thermal and pressure equilibrium at $T \lesssim 300 \, \mathrm{K}$ and $T \approx 8000 \,\mathrm{K}$ (e.g., Shull & Woods 1985 and references therein); astrophysicists somewhat casually call these states "phases", although these states do not differ in their degree of symmetry like phases defined in physics do. As long as the gas stays in thermal equilibrium or the temperature changes on timescales longer than the relevant ionization and recombination timescales, ionization equilibrium will appear. However, even in these cases, possible heating mechanisms like collisions of ions with Cosmic Rays or photons not only compensate the radiative cooling due to collisions of ions and thermal electrons but also directly change the ionization states. Therefore both the radiative cooling rate and the total radiative energy-loss rate at equilibrium temperature differ from those of a gas in CIE at the same temperature.

Moreover, density or pressure disturbances of such stable gas phases can produce gas in transient states before reaching another equilibrium temperature. Estimates of timescales for these phase transitions have been discussed, for instance, in time-dependent models for the interstellar medium by Gerola et al. (1974). However, detailed quantitative calculations of these phase transitions and their integrated times in the interstellar gas have been published—to our knowledge—only by Biermann et al. (1972). It is obvious that these transient states of the gas cannot be described in terms of CIE. Recently, phase transitions in the broad line emission region of active galactic nuclei have

² Institut für Theoretische Astrophysik der Universität Heidelberg, Im Neuenheimer Feld 561, W-6900 Heidelberg 1, Germany

been investigated by us. We calculated the real length of time for shock-induced phase transitions, using the same thermally self-consistent time-dependent code (HOTGAS) which T.S. developed for the calculations presented in this paper. First results are given in Schmutzler & Tscharnuter (1992).

There also exist gas components in the disk and halo of our Galaxy with temperatures of 10⁵ K to 10⁶ K (Cox 1991, Savage 1991). We do not know any global permanent heating mechanism to keep this gas in thermal equilibrium within this wide temperature range. So it is more likely that we just observe the gas in a transient state. Then, as a consequence of its inherent properties, the gas must be out of ionization equilibrium; at least out of collisional ionization equilibrium. The origin of this component can be explained by shock-heating up to 10⁶–10⁷ K by supernova explosions and expansion of their remnants. The galaxy M 82 for example demonstrates this heating mechanism in a very impressive fashion (Schaaf et al. 1989).

These arguments show that the ionization states, the energy-loss rate and hence the cooling curve gained from CIE calculations are in many cases only a first approximation and sometimes obviously a bad one. A better description is also needed for theoretical simulations, for example in modelling the chemical and gas dynamical evolution of galaxies (Hensler & Burkert 1990). Within this context the thermal and dynamical evolution of interstellar gas and its dependence on different aspects, such as metallicity or locally acting radiation fields, will now be of especial interest (Böhringer & Hensler 1989). Our understanding of intergalactic gas, cooling flows and the physics in AGNs will also profit by detailed self-consistent time-dependent calculations of thermal processes.

In this paper we concentrate on the more general aspects of radiatively cooling gases and present time-dependent radiative cooling rates, ionization states and cooling timescales to compare with those of a gas in CIE. Emission spectra of time-dependent cooling gases and applications in special environments, like phase transitions in the emission line regions of AGNs, will be discussed in forthcoming papers.

Our calculations are restricted to a purely atomic gas, optically thin to its own photon emission with two exceptions for hydrogen. We follow the evolution of a small gas volume and consider the physical processes per cm³. In comparison with the work of Shapiro & Moore (1976) we use more recent atomic data and include some more physical processes like excitationautoionization, charge exchange and two-photon emission. In addition, as an important extension of physical processes, we allow for special studies the interaction with an external photon field. We then include photoionization, Auger effect, Compton scattering and secondary ionization. Our cooling function contains 1155 line transitions (permitted, forbidden and semiforbidden ones) in the spectral range from far infrared to X-ray as well as the continuum processes, i.e. two-photon emission, recombination, collisional ionization, bremsstrahlung, and—if necessary, inverse Compton scattering. Our definition of the internal energy considers not only hydrogen but also all elements and ionization stages. Thus we set up a self-consistent system of ordinary differential equations which we solve by an implicit method. The great advantage of this approach is the flexibility to follow any given thermodynamical path.

The physical processes and the sources of the employed atomic data are briefly described in the next section. We show the basic equations in Section 3, discuss the mathematical method in Section 4, and present our results in the last section.

2. Physical processes and atomic data

Here we present only a short list of the physical processes taken into account and the references for the atomic data used. A comprehensive description of the data can be found in Schmutzler (1987); a complete documentation of our code HOTGAS will be given in Schmutzler (1993).

We consider the ten most abundant elements H, He, C, N, O, Ne, Mg, Si, S and Fe. Ionization occurs by collisions with thermal electrons, charge exchange and photoionization. Hydrogen and helium can also be ionized by suprathermal electrons produced by high energy photoionization and the Auger effect (Shull 1979; Halpern & Grindley 1980; Binette et al. 1985). The rates for thermal ionization, including excitationautoionization and charge exchange, are taken from Arnaud & Rothenflug (1985). In addition to charge exchange (which also is a recombination process) we consider both types of direct recombination due to two-body collisions: radiative and dielectronic recombination, which is the inverse of excitationautoionization. Since we only treat thin gases, the probability of the inverse process to collisional ionization—that is three body recombination—is negligible. We use recombination coefficients including all possible recombinations into excited levels and into the ground level. However, for hydrogen we use the "on-the-spot"-approximation (Osterbrock 1974). The coefficients are taken from Tarter (1971), Shull & Van Steenberg (1982a, 1988b), Aldrovandi & Péquignot (1973, 1976) and Arnaud & Rothenflug (1985). Radiative recombination of helium, the second most abundant element, produces photons which are assumed to ionize hydrogen directly.

To investigate the influence of an external photon field, for example in the interstellar medium surrounding a luminous star or star association, we have taken into account the most important interactions of photons with atoms, ions and electrons. The total photoionization cross sections are taken from Reilman & Manson (1978, 1979). We have interpolated each of their tabulated cross sections in a series of power laws. The required subshell cross sections are derived from the total one. For hydrogen- and hydrogen-like ions in the 1-s state we use the exact cross section formula (e.g., Vogel 1972). If the photon energies are much higher than the ionization potential the extrapolated cross sections fall below the Thomson cross section. In these cases we follow the arguments of Halpern & Grindlay (1980) and calculate the Compton ionization cross sections for all ions.

High energy photons are more likely to ionize an inner shell than an outer one. If the ensueing reconfiguration of electrons makes sufficient energy available there is a certain probability of an additional emission of one or more of the outer electrons. This type of autoionization is the well known Auger effect. We use the probabilities and number of emitted electrons per inner shell ionization worked out by Weisheit (1974).

The energetics are balanced in detail by the most important radiative cooling processes as well as by transforming thermal kinetic into potential (ionized states) and, if necessary, external photon energy into internal (kinetic and potential) energy via ionization. We determine the energy-loss due to Coulomb collisions of electrons and ions using the formula of thermal bremsstrahlung (Novikov & Thorne 1973) with the frequency averaged Gaunt factor given by Karzas & Latter (1961). Both types of recombination transform thermal kinetic and potential energy into radiative loss. We derived the corresponding cooling rates from the total volume emissivity given by Cox & Tucker (1969). In case of dielectronic recombination we use the first excitation energies tabulated in Landini & Fossi (1971). However, the most important energy-loss results from collisional excitation followed by spontaneous line emission including two-photon continuum emission. In total we consider 1155 line transitions in the spectral range from 1Å to 610 μ . The data are based on the work of Kato (1976), Stern et al. (1978), Osterbrock (1963, 1971), Osterbrock & Wallace (1977), Jura & Dalgarno (1972) and Penston (1970). For more details see Schmutzler (1993).

If an external photon field illuminates the gas the appropriate heating terms due to photoionization, Compton ionization and Auger effect are taken into account. In addition we include the net energy exchange rate between photons and electrons due to Compton scattering (Levich & Sunyaev 1970, 1971).

3. The basic equations

A thermally self-consistent approach of radiatively cooling gas requires detailed balancing of energy, the time-dependent stages of ionization, charge conservation, the equation of state and a description of the gas dynamics, at least in a global way. We calculate the physical behaviour of our gas volume by simultaneously solving a system of 103 nonlinear ordinary differential equations together with 14 algebraic relations. The variables we use are the gas temperature T, pressure P, mass density ϱ , electron density per mass unit $\frac{n_e}{\varrho}$, ion density per mass unit $\frac{n_{Z,z}}{\varrho}$ and internal energy per mass unit U; here Z and z denote the nuclear and effective charge of an ion, respectively. Following the arguments given in Shapiro & Moore (1976), we assume an equal Maxwellian temperature for ions and electrons. For special studies of the physics in activ galactic nuclei Schmutzler & Lesch (1989) have shown that this assumption holds also in the case of very fast Compton-heating of electrons, for instance in the hot gas phase of the broad line and narrow line region of active galactic nuclei.

We list the basic equations without presenting all detailed terms in energy balance and time-dependent state of ionization. To find the effective length of time for cooling or heating we have to consider the gas in a more realistic description than just assuming an ideal monoatomic one whose internal energy is given only by the thermal translation energy. The reason is due to the fact that a huge amount of energy can be stored in or delivered from high ionization stages of the chemical elements. Therefore the total radiative energy-loss (or gain) is not in every case synchronized with an equivalent decrease (or increase) of temperature. Thus we employ for the energy balance the specific internal energy U defined by

$$U - \sum_{Z} \sum_{z=1}^{Z} \left(\frac{n_{Z,z}}{\varrho} \sum_{z'=0}^{z-1} I_{Z,z'} \right) - \frac{3}{2} \frac{P}{\varrho} = 0$$
 (1)

where $I_{Z,z'}$ gives the ionization potential of an ion with nuclear charge Z and effective charge z'. This definition implicitly considers the fact that the commonly used ratio of specific heats $\gamma = c_P/c_V$ is not a constant. In general, the internal energy also contains the sum over all populated excitation levels. In a thin gas, however, the assumption of instantaneous decay is an excellent approximation, since the timescales of line transitions, even of forbidden ones, are much shorter than all other important timescales. Therefore we neglect this sum in the definition of the internal energy and consider collisional excitation only in the net cooling term. The equation of energy balance now reads:

$$\frac{dU}{dt} - \frac{P}{\varrho} \frac{d \ln \varrho}{dt} + \frac{\mathscr{L} - \mathscr{G}}{\varrho} = 0.$$
 (2)

The net radiative cooling rate $\mathcal{L}-\mathcal{G}$, expressed by the cooling function \mathcal{L} and a possible heating function \mathcal{G} , represents only that part of the total radiative energy-loss which couples to the thermal evolution of the gas. It depends on temperature, electron density and ionization states. Moreover, the contribution of an external photon field depends on photon density and energy spectrum. Ion and electron densities are determined by ionization and recombination rates, which also depend on temperature, particle densities and external photon field. Thus we have to solve 102 ordinary differential equations balancing the ionization states of all ions ($z \neq 0$) given in the form:

$$-\frac{d\left(\frac{n_{Z,z}}{\varrho}\right)}{dt} + \frac{1}{\varrho} F_{Z,z}(T, n_e, n_{Z,z}, \tilde{n}_{\tilde{Z},\tilde{z}}, \zeta_{Z,z}^{\text{phot}}) = 0.$$
 (3)

The functions $F_{Z,z}$ contain all ionization and recombination rates which, due to charge exchange, may also depend on the particle density of other ions $\tilde{n}_{\tilde{Z},\tilde{z}}$. The dependence on possibly interacting photons is indicated by $\zeta_{Z,z}^{\text{phot}}$.

To illustrate which kind of functions the $F_{Z,z}$ are we show as an example the function for hydrogen (Z = 1, z = 1):

$$F_{1,1} = \left(\xi_{1,0} + \left(\alpha_{2,1} \, n_{2,1} + \alpha_{2,2} \, n_{2,2}\right) \frac{n_{\rm e}}{N_2}\right) \, n_{1,0} -$$

$$- \alpha_{1,1} \, n_{\rm e} \, n_{1,1}$$
(3.1)

with N_2 denoting the total particle density of helium atoms and ions. As mentioned above, here we assume that recombination of helium causes ionization of hydrogen. In general the total

ionization rates and recombination coefficients are given by the following sums (Eqs. (3.2) and (3.3), respectively):

$$\xi_{Z,z} = \zeta_{Z,z}^{\text{phot}} + \left(C_{Z,z}^{di}(T) + C_{Z,z}^{ea}(T) \right) n_{\text{e}} +$$

$$+ \zeta^{\text{e}} + \sum_{z} C^{ce}(T) \tilde{n}_{\tilde{Z},\tilde{z}}$$
(3.2)

where $\zeta_{Z,z}^{\mathrm{phot}}$ denotes the total or special subshell photoionization rate, $C_{Z,z}(T)$ the thermal collisional ionization rates and $C^{ce}(T)$ the ionization rate due to charge exchange. The upper indices stand for direct (di) and excitation-autoionization (ea). The ionization rate due to suprathermal electrons ζ^{e} is taken into account only for H and He, whereas $C_{Z,z}^{ea}(T)$ contributes only to some special metal ions. The recombination coefficients are

$$\alpha_{Z,z}(T) = \alpha_{Z,z}^r(T) + \alpha_{Z,z}^d(T) + \frac{1}{n_e} \sum_{z} \alpha^{ce}(T) \tilde{n}_{\tilde{Z},\tilde{z}} .$$
 (3.3)

Here the upper indices stand for radiative, dielectronic and charge exchange processes, respectively. Of course, for hydrogen we have $\alpha^d = 0$.

The abundances of atoms (z = 0) then can be found using the 10 equations which also fix the relative chemical abundances X_Z in a gas with changing mass density:

$$\sum_{z} \frac{n_{Z,z}}{\varrho} - \frac{X_Z}{\langle \mu \rangle} = 0 \tag{4}$$

where $\langle \mu \rangle$ denotes a normalized mean mass for a given chemical composition. Charge conservation determines the electron density:

$$\sum_{Z,z} \frac{n_{Z,z}}{\varrho} z - \frac{n_{\rm e}}{\varrho} = 0. \tag{5}$$

Pressure, temperature and mass density are tied in the equation of state:

$$P - \varrho \left(\sum_{Z,z} \frac{n_{Z,z}}{\varrho} + \frac{n_{\rm e}}{\varrho} \right) kT = 0.$$
 (6)

Finally, in order to take into account the dynamics in a global way, we have to fix one additional relation, for example, the time variation of the pressure (or density or temperature) according to the timescales of the physical scenario of interest:

$$P - f(t) = 0 \tag{7}$$

Two of the simplest assumptions are for example an isobaric or isochoric evolution. Then Eq. (7) reads $P-P_0=0$ or $\varrho-\varrho_0=0$, respectively.

4. Mathematical method

This system of 103 coupled ordinary differential equations (together with 14 algebraic relations) is well known to be a stiff one, since it covers a wide spectrum of relevant timescales ranging over more than 6 orders of magnitude. Such stiff systems of differential equations require an implicit method for an efficient solution. We choose a Newton iteration which is known to be a powerful and stable method, see for example the discussion in Byrne & Hindmarsh (1987).

We point out that we calculate the complete rate matrix, since we allow for charge exchange and, when photoionization is taken into account, for multiple ionization due to the Auger effect. Therefore, we cannot use algorithms which have been worked out for tridiagonal matrices.

We start with arbitrary initial values and approximate the time derivations in Eqs. (2) and (3) by their difference quotients, typically using a timestep of one tenth of the estimated cooling timescale as "natural" guess. Then we check whether the total system of equations is fulfilled and iterate, if necessary, by determining the Jacobian matrix and calculating the corrections with a Gauss elimination method. In mathematical symbols we have to find all δx_k solving the i equations:

$$G_i(x_1^{(n)}, ..., x_m^{(n)}) + \sum_{k=1}^m \left(\frac{\partial G_i}{\partial x_k}\right) \delta x_k = 0.$$
 (8)

In our case index i runs from 1 to m = 117. The derivatives in

$$\left(\mathbf{J}_{k}^{i}\right) \equiv \left(\frac{\partial G_{i}}{\partial x_{k}}\right) \tag{9}$$

are computed numerically, i.e., $\left(\partial G_i/\partial x_k\right)\approx \left(\Delta G_i/\Delta x_k\right)$, to find

$$\delta x_k = -\left(\mathbf{J}_k^i\right)^{-1} G_i(x_1^{(n)}, ..., x_m^{(n)}) \tag{10}$$

which yields the next better approximation

(6)
$$x_k^{(n+1)} = x_k^{(n)} + \delta x_k$$
. (11)

We proceed as long as $\delta x_k/x_k^{(n)}<10^{-5}$ for all k and $G_i(x_1^{(n)},...,x_m^{(n)})/x_i<10^{-5}$ for all i in two subsequent iterations. In most cases five or six iterations give an accuracy better than 10^{-8} . If there is no good convergence we repeat with the halfwidth of the timestep or, if necessary, with a quarter or an eighth of the last one, respectively. The timestep increases again if the convergence is good and if the relative change of the variables is less than 5%. In the most extreme case the timestep was found to be $\approx 2.4\,10^{-4}$ of the guessed one, but rapidly increased again by consecutive factors of 2 to the "natural" upper limit.

5. Results and discussion

We restrict the discussion in this paper to the evolution of a gas volume due to its inherent physical properties and neglect all interactions with its environment which have to be considered in detailed models of the interstellar medium or supernova remnants (e.g., Hughes & Helfand 1985; Gaetz et al. 1988). Otherwise it would be difficult to separate the internal physics and the influence from outside.

Unless otherwise specified the calculations we discuss use the cosmic abundances given by Allen (1973). To demonstrate the strong deviations between CIE and time-dependent calculations, and to faciliate comparison with previously published work, detailed results for an isochoric evolution and for a gas in CIE are given in Figs. 1–3. In this context we make particular reference to the excellent discussion on isochorically cooling gas and its applications to the interstellar medium given by Shapiro & Moore (1976, 1977). In addition we investigate the isobaric case, but we will discuss the main differences between isochoric and isobaric cooling by concentrating on some specific aspects.

We started both runs, the time-dependent one and the gas in CIE, at the same initial conditions with $T=10^9~\rm K$. In this initial state collisional ionization equilibrium for a fully ionized gas can safely be assumed. In the time-dependent run the gas then cools isochorically ($\dot{\varrho}=0$, no heating: $\mathscr{G}=0$ in Eq. 2) with a hydrogen number density $N_{\rm H}=1~\rm cm^{-3}$. Though the calculations range from $10^9~\rm K$ to $10^2~\rm K$ we compare in Figs. 1.1–1.18 the ionization stages of all elements only in the most interesting temperature intervals. The ionization stages are plotted as ratio of the ion density $n_{Z,z}$ to the total particle density of that chemical element N_Z .

Most of the differences between our results and those of Shapiro & Moore (1976) are due to the use of new atomic data and to the inclusion of the additional physical processes mentioned in the introduction. These affect both the CIE calculation and the time-dependent one. Especially for the time-dependent case, the different cooling rate and the self-consistent energy balance we use leads to deviations from previous results. Nevertheless, we find the general tendency of delayed recombination—which is especially pronounced for helium-like and neon-like ions and was pointed out by Kafatos (1973) and Shapiro & Moore (1976)—to be in a fair conformity with our results. The recombination at lower temperatures clearly has interesting consequences for the corresponding emission spectra, which we will present in a forthcoming paper.

The different ionization stages in the time-dependent case obviously lead to different line excitation and hence to a different radiative cooling rate. To show the composition of the radiative energy-loss, we first present in Fig. 2.1 the cooling rates of the time-dependent run due to the individual processes and then compare the normalized total cooling rates Λ of both calculations in Fig. 2.2. The individual processes are collisional ionization (C), radiative (R) and dielectronic (D) recombination, free-free emission (F) and collisional excited line (L) emission including two-gamma emission. To avoid an overrepresentation of the energy-loss by processes which do not depend on

Ionization fraction of Hydrogen

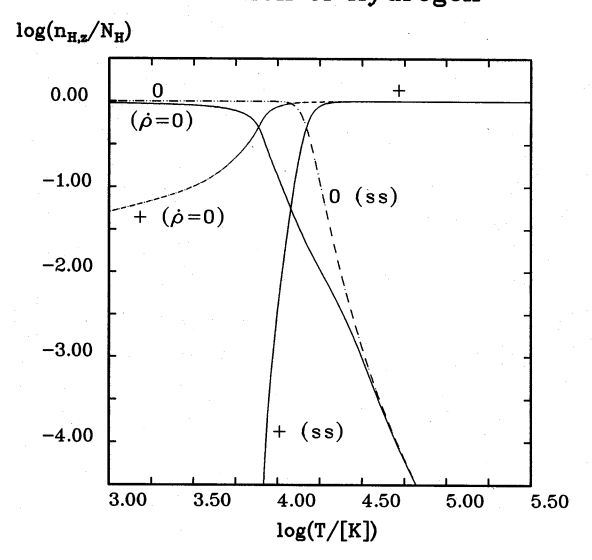


Fig. 1.1. Comparison of hydrogen ionization stages during isochoric $(\dot{\varrho} = 0)$ cooling and under the steady state assumption (ss), i.e., CIE

Ionization fraction of Helium

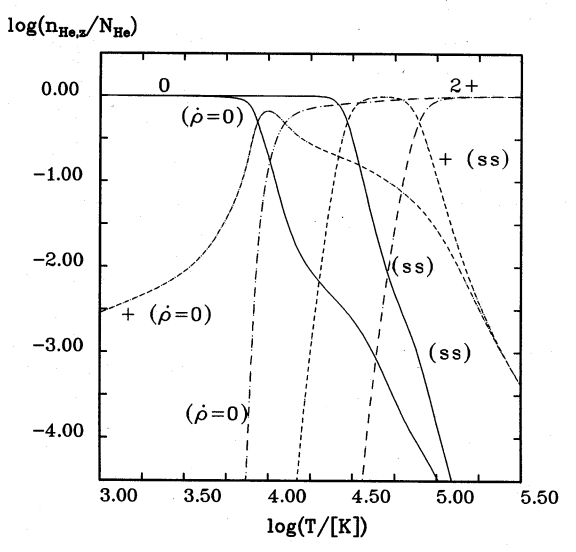


Fig. 1.2. Comparison of helium ionization stages during isochoric $(\dot{\varrho} = 0)$ cooling and under the steady state assumption (ss), i.e., CIE

the electron density like neutral-neutral line excitation, we have normalized Λ by $N_{\rm H}^2$ instead of the commonly used normalization factor proportional to $n_{\rm e}$. The units of Λ are ${\rm erg\,cm^3\,s^{-1}}$. Thus, in our notation the power per unit volume, only due to the cooling part of the radiation, is given by $\mathscr{L}=\Lambda\cdot N_{\rm H}^2$.

We find that the CIE result overestimates the effective cooling rate by factors of up to 7. Especially the peak of hydrogen Ly α at $T=1.74\ 10^4$ K vanishes in the time-dependent cooling rate because hydrogen cannot recombine efficiently at this temperature. As a consequence the delayed recombination due to the fast cooling itself reduces the energy-loss. Nevertheless,

Ionization fraction of Carbon

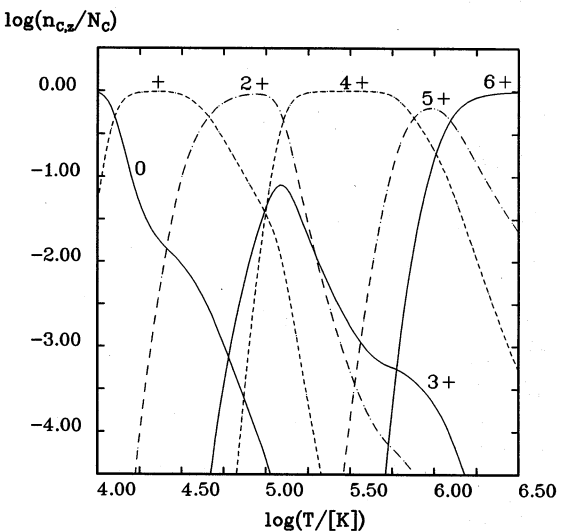


Fig. 1.3. Ionization stages assuming steady state (ss), i.e., CIE

Ionization fraction of Carbon

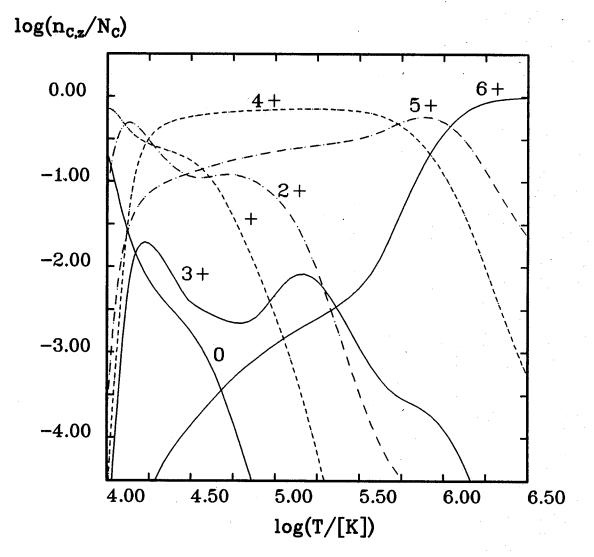


Fig. 1.4. Ionization stages during isochoric cooling ($\dot{\varrho} = 0$)

the cooling timescale remains shorter than the most relevant recombination timescales.

A comparison with results of other authors, for instance the isobaric cooling function (Fig. 5 in Gaetz et al. (1988)), shows a general agreement. However, there are differences in detail which relate either to the use of different data sets and abundances, or different rate approximations, or different concepts.

In the literature one often finds an estimate of the cooling time using the cooling rate of a gas in CIE. We note that this can be only a first approximation to find the right order of magnitude. In fact the cooling timescale can directly be derived from the cooling rate Λ (i.e., $t_{\rm c} \approx \frac{3}{2} nkT/(\Lambda \cdot N_{\rm H}^2))$ only within such temperature ranges where the internal energy is dominated by its thermal "kinetic" part $\frac{3}{2}\frac{P}{\varrho}$. In our calculation this applies

Ionization fraction of Nitrogen

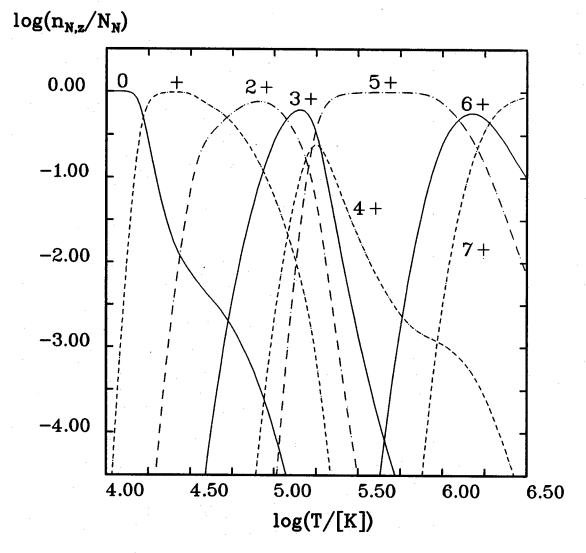


Fig. 1.5. Ionization stages assuming steady state (ss), i.e., CIE

Ionization fraction of Nitrogen

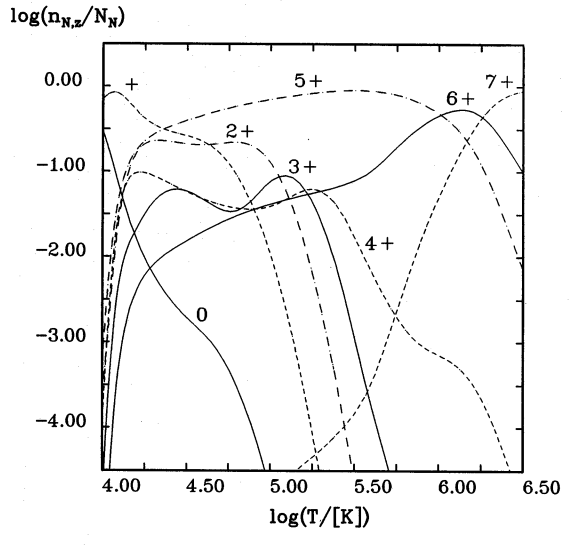


Fig. 1.6. Ionization stages during isochoric cooling ($\dot{\varrho} = 0$)

for temperatures above a few 10^5 K. At lower temperatures the radiative cooling rate does not lower the temperature simultaneously, since the internal energy contains additional degrees of freedom which have to be reconfigured. In addition a huge reservoir of potential energy is stored by the high ionization stages of the elements. In fact, at a temperature of $T = 10^4$ K we find that the potential energy exceeds the thermal kinetic part by more than a factor of 5. Of course, this factor depends on the metallicity. In any case, at these temperatures a redistribution of internal energetics rather than a direct cooling of the gas is a consequence of the delayed recombination at higher temperatures. The accompanying radiative energy-loss (recombination continuum) should in principle be detectable in the UV

Ionization fraction of Oxygen

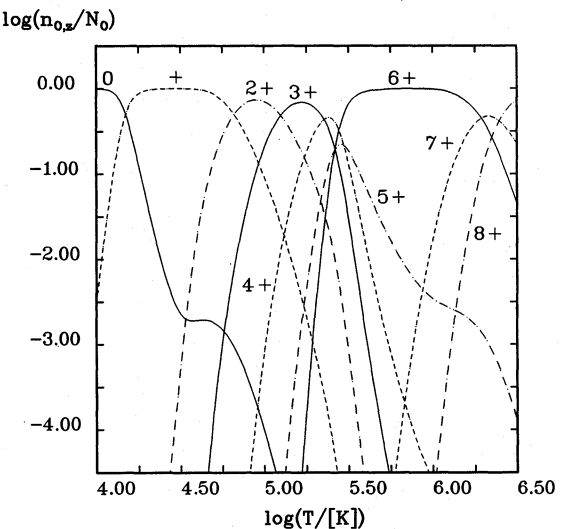


Fig. 1.7. Ionization stages assuming steady state (ss), i.e., CIE

Ionization fraction of Oxygen

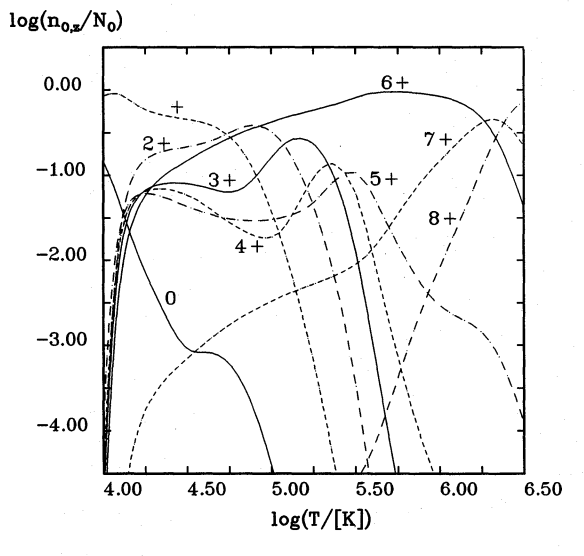


Fig. 1.8. Ionization stages during isochoric cooling ($\dot{\varrho} = 0$)

and soft X-ray ranges (Schmutzler & Tscharnuter, in preparation). Another aspect of this behaviour can be seen in the ratio of specific heats $\gamma = c_P/c_V$, which approaches unity. However, in the context we are discussing here, this "adiabatic index" has no physical meaning except that it might be one additional measure of the deviation from an ideal gas without internal degrees of freedom.

The cooling timescale is given by |T/(dT/dt)|, whereas the exact cooling time can be found only by complete integration from the initial temperature to the final one. However, as long as the gas starts to cool at temperatures $T>10^7~\rm K$ the cooling time is dominated by the cooling timescale of this high temperature. Within about two timescales our gas volume cools to $100~\rm K$ or less, neglecting all possible interactions with sur-

Ionization fraction of Neon

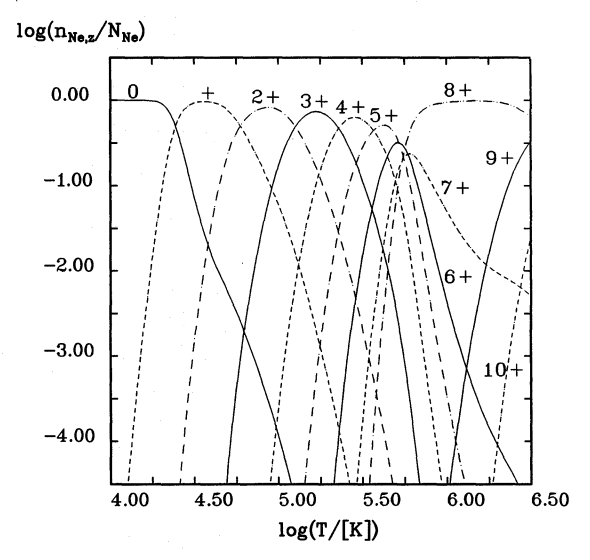


Fig. 1.9. Ionization stages assuming steady state (ss), i.e., CIE

Ionization fraction of Neon

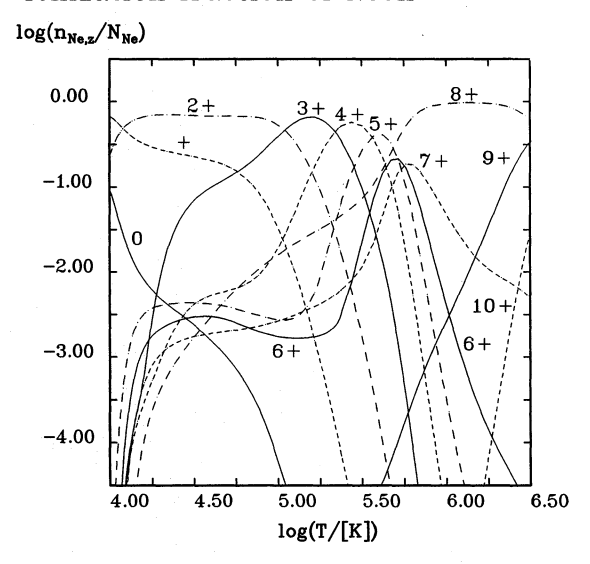


Fig. 1.10. Ionization stages during isochoric cooling ($\dot{\rho} = 0$)

rounding gas volumes. Of course, this will change if a heating source reduces the net cooling. At lower temperatures the ratio of the integrated times for cooling to 100 K and the cooling timescale increases dramatically; we find the following ratios: 27 at 10^6 K, 400 at 10^5 K, 131 at 10^4 K and 16 at 10^3 K. The cooling curve $|N_{\rm H}^{-1}(dT/dt)|$ versus T of an isochorically cooling gas is shown in Fig. 3. This curve relates to the evolution of gas temperature rather than the cooling rate. The different shapes of the cooling curve and the radiative cooling rate at temperatures around 10^4 K again demonstrate the importance of a self-consistent energy balance.

In the case of isobaric cooling the gas density increases with decreasing temperature. Thus the absolute timescales t are

Ionization fraction of Magnesium

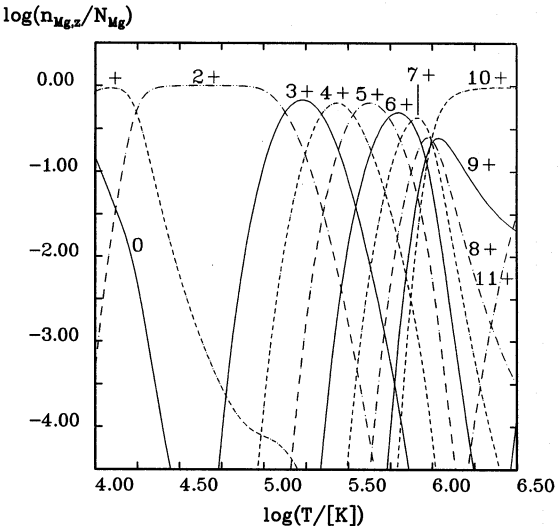


Fig. 1.11. Ionization stages assuming steady state (ss), i.e., CIE

Ionization fraction of Magnesium

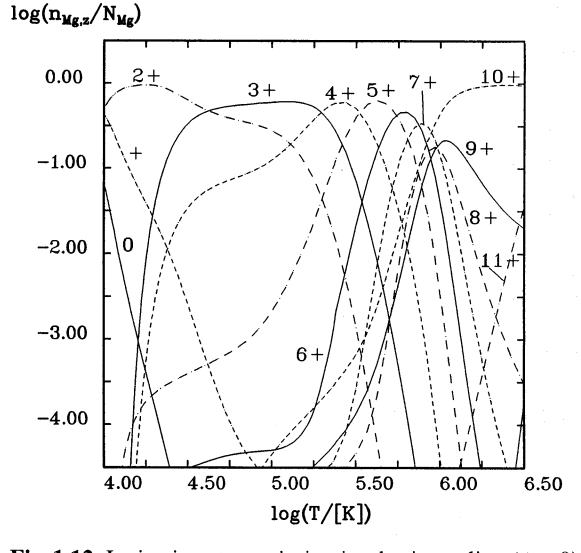


Fig. 1.12. Ionization stages during isochoric cooling ($\dot{\varrho} = 0$)

shorter than for isochoric cooling, because $t \propto n^{-1}$. Since all relevant atomic processes are proportional to the product of ion number density times electron number density and to functions of temperature, the ratios of the corresponding timescales are not affected by the increase of density. At first glance, if atomic processes only are considered, the derived ionization stages and energy-loss rate as functions of temperature would be the same as for isochoric cooling. However, the energy equation (Eq. (2)) for isobaric cooling differs by the term $-\frac{P}{\varrho} \frac{d \ln \varrho}{dt}$. This term describes the energy input due to the compressional work on the gas, which of course vanishes in the isochoric case. The redistribution of internal energy now affects the ionization stages as well as the radiative cooling and energy-loss rate.

Ionization fraction of Silicon

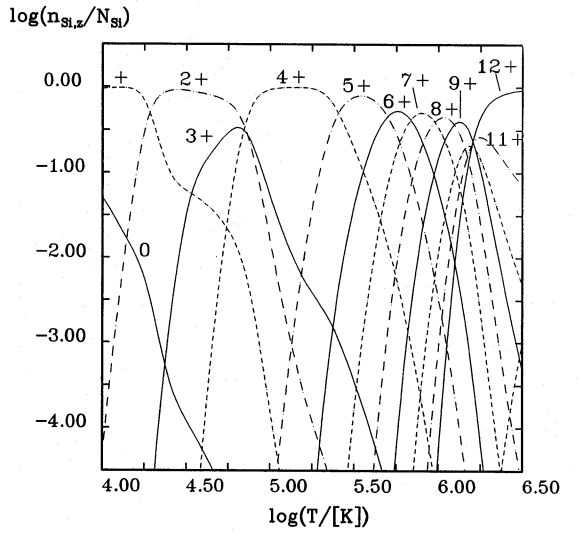


Fig. 1.13. Ionization stages assuming steady state (ss), i.e., CIE

Ionization fraction of Silicon

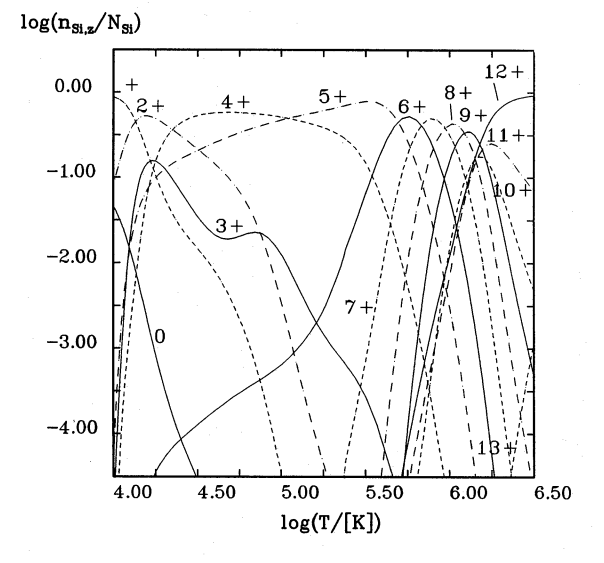


Fig. 1.14. Ionization stages during isochoric cooling ($\dot{\varrho} = 0$)

We started an isobaric run at $T = 10^9$ K with $N_{\rm H} = 1$ cm⁻³ and indeed found clear differences to the isochoric case. However, these are not as significant as the differences between CIE and time-dependent cooling. We illustrate the differences between the isochoric and isobaric case by comparing the ionization stages of hydrogen and helium in Figs. 4.1 and 4.2; the corresponding radiative cooling rates are compared in Fig. 5.

So far we have given an overview on the evolution of a cooling gas following two of the basic thermodynamical pathes and have presented the most important aspects like ionization stages and cooling rates. In the next section we discuss some further details in more depth.

Ionization fraction of Sulfur

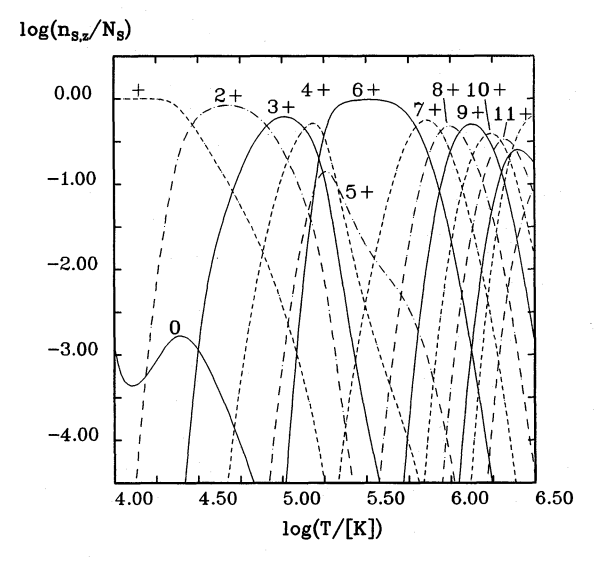


Fig. 1.15. Ionization stages assuming steady state (ss), i.e., CIE

Ionization fraction of Sulfur

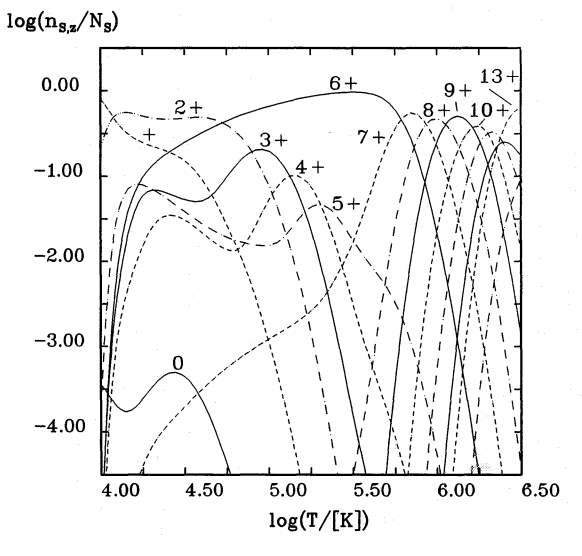


Fig. 1.16. Ionization stages during isochoric cooling ($\dot{\varrho} = 0$)

5.1. The rôle of the previous ionization state

Since the ratios of the relevant intrinsic timescales in a radiatively cooling gas, at least in the temperature range $T \leq 510^6$ K, lead to nonequilibrium ionization, both the ionic abundances and the corresponding energy-loss rate are not only functions of the temperature but also of the history of the gas. This means, for instance, that the initial ionization state and the corresponding electron density determine the temporal evolution of the gas as well as the initial temperature. Therefore the nature of a previous heating mechanism influences the cooling. Shapiro & Moore (1976) have demonstrated and discussed this effect in a few examples for shock-heated gas with a low degree of ionization and for previously photoionized gas. We will not present our results here, since their general behaviour is similiar to pre-

Ionization fraction of Iron

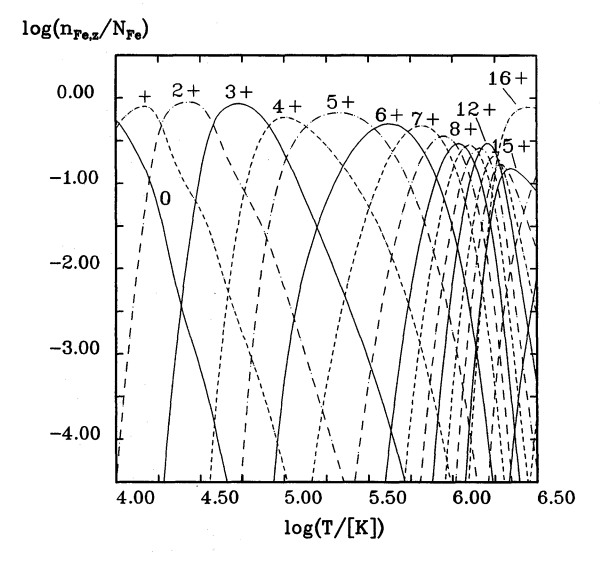


Fig. 1.17. Ionization stages assuming steady state (ss), i.e., CIE

Ionization fraction of Iron

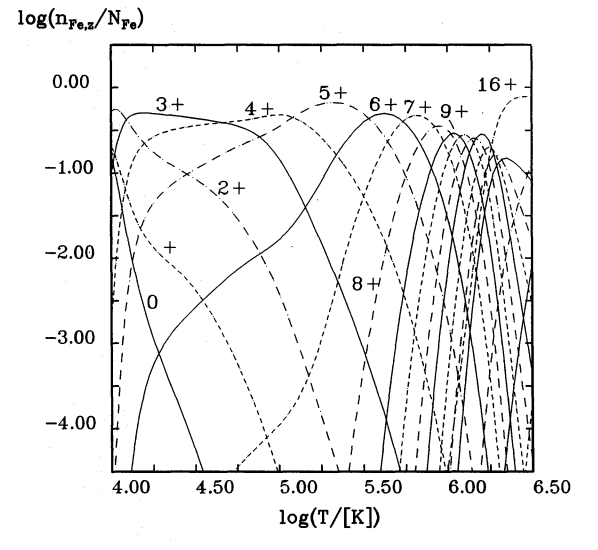
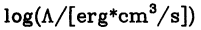


Fig. 1.18. Ionization stages during isochoric cooling ($\dot{\varrho} = 0$)

vious work. The differences are once again attributable to our different atomic data and physical processes as well as to our more complete energy equation. Nevertheless, we will report one of our most extreme examples.

We have assumed a nearly neutral gas with $n_{\rm e}/N_{\rm H}=6.5\ 10^{-6}$ which cools isochorically (with $N_{\rm H}=1\ {\rm cm}^{-3}$) after shock-heating to a temperature of $T=5\ 10^5$ K. At this temperature the radiative cooling rate is in the maximum range for CIE and for time-dependent cooling from higher temperatures. Then line excitation of highly ionized C, N and O dominates the energy loss. By contrast, the radiative cooling within the first 210^8 s for our special case is caused by lines in the infrared spectral range, excited by neutral-neutral collisions, Ly α -emission of hydrogen, and ionization processes. Ionization does not decrease

The Cooling Rates



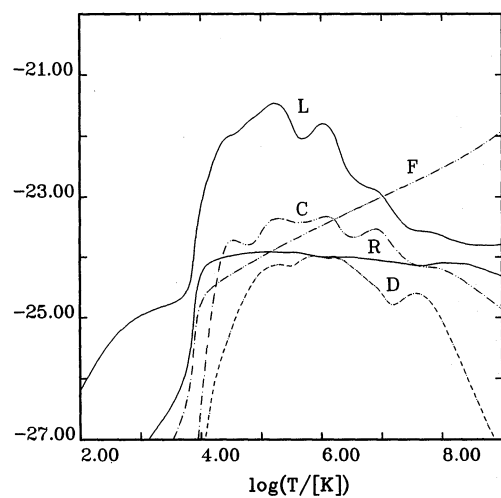


Fig. 2.1. The radiative cooling rates due to the individual processes during iochoric cooling ($\dot{\varrho}=0$); C, R, D, F and L stands for collisional ionization, radiative and dielectronic recombination, free-free emission and collisionally excited line emission including two-gamma emission. respectively

Total Cooling Rate

$\log(\Lambda/[erg*cm^3/s])$

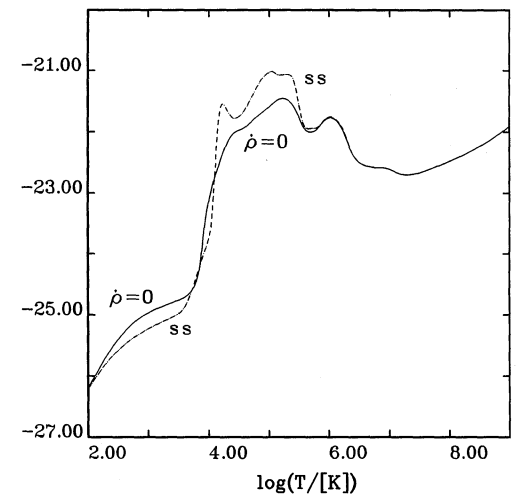


Fig. 2.2. Comparison of the total radiative cooling rate during isochoric cooling ($\dot{\varrho} = 0$) and under the steady state assumption (ss), i.e., CIE

the internal energy, but cools the gas. As soon as the electron density has been grown to a few percent of the hydrogen number density, collisional excitation of hydrogen $Ly\alpha$ -emission starts to dominate the energy-loss rate. It now exceeds the cooling rate of an ionized gas cooling from higher temperatures (cf., Fig. 2) by more than three orders of magnitudes. The cooling becomes much faster than the rate at which hydrogen can be ionized. Therefore the degree of ionization remains below 43%. The heavier elements, too, remain in neutral or singly ionized stages and the gas cools within $8.5\,10^{11}$ s to about 10^4 K. The compara-

Cooling Curve

$\log(|N_H^{-1}dT/dt|/[cm^3K/s])$

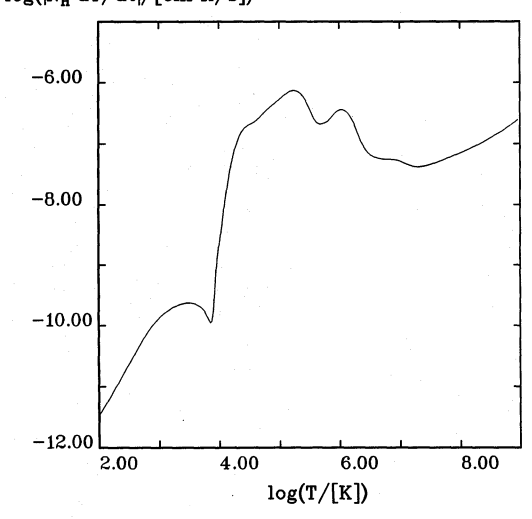


Fig. 3. The cooling curve of a isochorically cooling gas $(\dot{\varrho} = 0)$

Ionization fraction of Hydrogen

$log(n_{H,z}/N_H)$

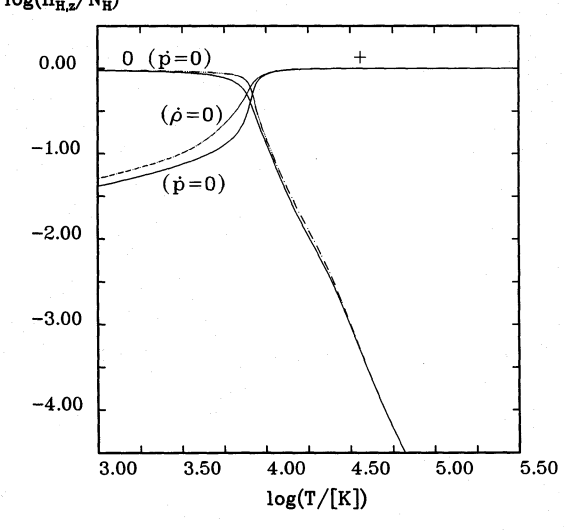


Fig. 4.1. Comparison of hydrogen ionization stages of an isochorically $(\dot{p} = 0)$ and an isobarically $(\dot{p} = 0)$ cooling gas

ble cooling time calculated in the run presented in the beginning of Sect. 5. is about 10^{13} s. This type of evolution shows drastically the consequence of the very low electron density in the beginning. We note that we have chosen this example rather to demonstrate the importance of the history of the gas than to model a realistic situation. For instance, we did not take into account the possibility of ionization via neutral-neutral collisions which again would introduce some more timescales. Moreover, shocks in astrophysical environments are often accompanied by photons which may previously photoionize the gas before the shock energy is converted into heat (Morrison & Sartori 1969). The first photon flash, produced by a supernova explosion, for

Ionization fraction of Helium

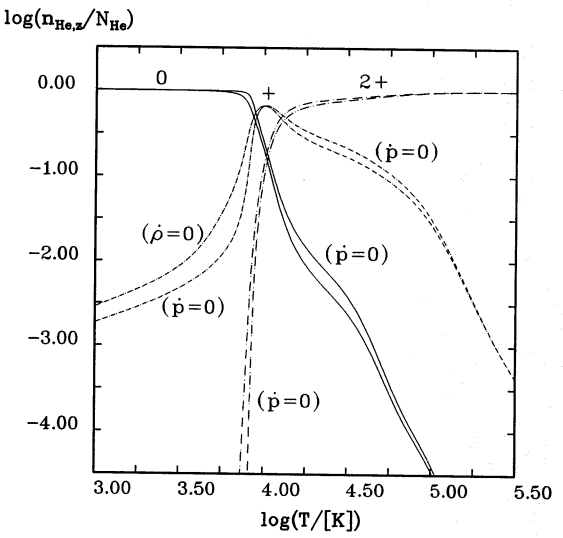
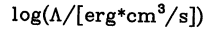


Fig. 4.2. Comparison of helium ionization stages of an isochorically $(\dot{p} = 0)$ and an isobarically $(\dot{p} = 0)$ cooling gas

Total Cooling Rate



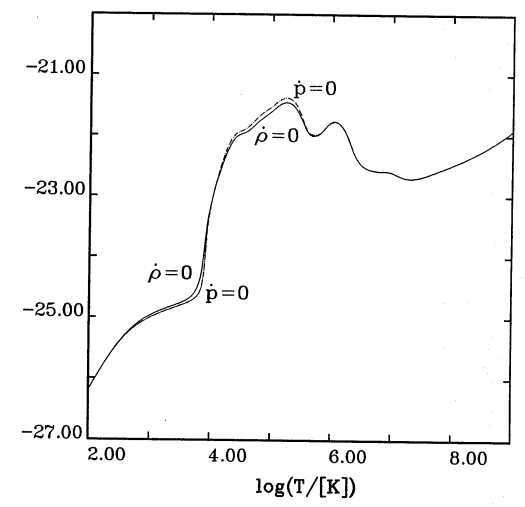


Fig. 5. Comparison of the total radiative cooling rates of an isochorically $(\dot{p} = 0)$ and an isobarically $(\dot{p} = 0)$ cooling gas

instance, then is followed by the precursing photons emitted by gas shock-heated in the downstream region.

5.2. Basic applications to the interstellar medium

5.2.1. The metallicity dependence

The dependence of the cooling rate in CIE on metallicity has been shown by Schmutzler (1987) and in more detail by Böhringer & Hensler (1989). In the case of time-dependent cooling gas the metallicity affects the cooling rate in a more complicated way. Of course, the ionization stages at certain temperatures depend on the effective cooling rate which is dominated

Total Cooling Rate

 $log(\Lambda/[erg*cm^3/s])$

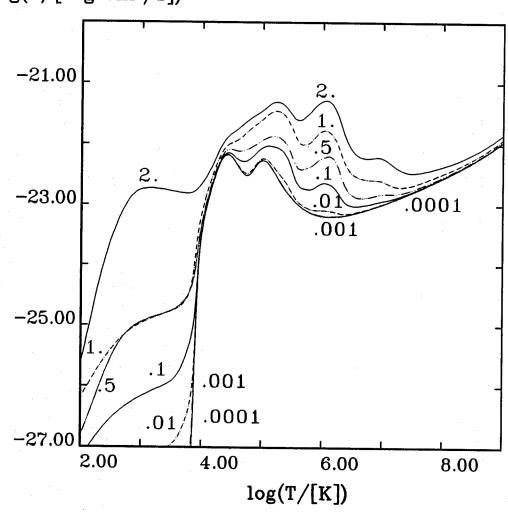


Fig. 6. The total radiative cooling rates of isochorically ($\dot{\varrho} = 0$) cooling gases with different metallicities; the curves are labeled due to the abundances of elements Z heavier than helium, normalized to the cosmic abundances of Allen (1973)

by line cooling and therefore is a function of the metallicity, but again the radiative cooling rate itself depends on the ionization states. In a series of calculations we investigated the dependence of the cooling rate on metallicity. In each case we assumed a gas cooling isochorically starting from CIE at $T = 10^9$ K, but with different abundances of elements Z heavier than helium given by the ratio \mathbb{Z}/\mathbb{Z}_c , where \mathbb{Z}_c denotes the cosmic abundances (Allen 1973). The results are plotted in Fig. 6, where the curves are labeled with Z/Z_c ranging from 2 to 10^{-4} . Since the radiative cooling rate and the cooling timescale depend on the metallicity, whereas this dependence is only a weak one for the ionization and recombination timescales due to charge exchange reactions, the departure from CIE calculations increases with increasing metallicity. For instance, the fast cooling due to the enrichment of heavy elements by a factor of 2 (Fig. 6) leaves ionized elements at temperatures far below 104 K. The appropriate line excitations (infrared lines) increase the cooling rate at these temperatures by more than two orders of magnitude in comparison with a gas with cosmic abundances.

5.2.2. Interaction with a photon field

For the gases we discussed so far, we have assumed only radiative cooling without any influence from the environment, except for the case of isobaric cooling. Here, per definition, the cooling gas volume is assumed to be compressed by the surrounding matter. Of course, in the interstellar medium (ISM) the situation is generally somewhat different. Besides the real hydrodynamical behaviour, for instance, there also is a radiation field interacting with the ISM. From these photons one should expect at least a small effect due to photoionization as well as from modifying the net cooling rate by the corresponding energy-gain ($\mathscr{G} > 0$ in Eq. 2). In the case of a very dilute

External Spectrum

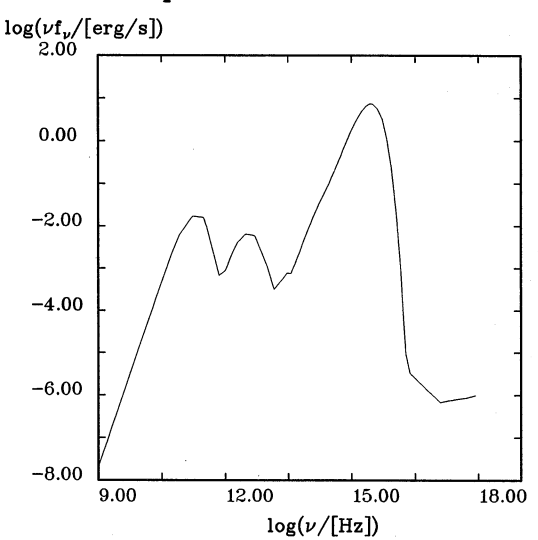


Fig. 7. Energy spectrum of an assumed photon field to heat a cooling gas; for explanation see text in Sect. 5.3

Total Heating and Cooling Rates

 $log(\Gamma)$; $log(\Lambda)$

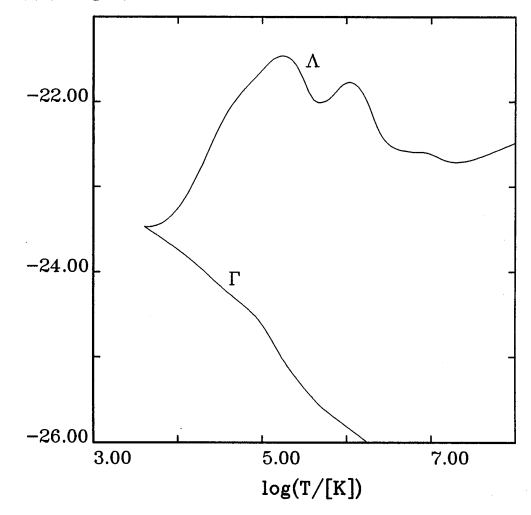


Fig. 8. The total radiative cooling rate $\Lambda = \mathcal{L}/N_{\rm H}^2$ of an isochorically $(\dot{\varrho}=0)$ cooling gas which is heated by the external photon field with energy spectrum displayed in Fig. 7; the lower curve represents the corresponding heating rate $\Gamma = \mathcal{L}/N_{\rm H}^2$, mainly due to photoionization. See text in Sect. 5.3

gas even the mean interstellar radiation field, for instance that at the Sun's location, should have some influence on atoms and ions with low ionization potentials. The ionization parameter Ξ , given by the ratio of the pressure of the ionizing photons to the thermal pressure, allows a first check for the gas temperature and density ranges in which the photon flux becomes energetically important. The ionization parameter $\Xi = (F_{\rm ion}/c)(nkT)^{-1}$ was introduced in this form by Krolik, McKee and Tarter (1981).

However, the strong UV-photon field of an O-, B-star association may affect Although the total flux of the mean interstellar

photon spectrum at the Sun's location is $F \simeq 8 \ 10^{-2} \ {\rm erg \, s^{-1}}$ (Black 1987), the ionizing flux is only a small fraction $F_{\rm ion} \simeq 1.5 \ 10^{-5} \ {\rm erg \, s^{-1}}$, or $F_{\rm ion} \simeq 1.1 \ 10^{-3} \ {\rm erg \, s^{-1}}$, depending on whether one considers the UV-gap (caused by observational reasons) in the spectrum or not. From these fluxes and the shape of the spectrum one expects a significant influence on the cooling process only for temperatures far below $10^4 \ {\rm K}$ and for very dilute gases ($n < 10^{-3} \ {\rm cm^{-3}}$ or $n < 10^{-2} \ {\rm cm^{-3}}$, respectively).

However, the strong UV-photon field of an O-, B-star association may affect the radiative cooling of neighbouring gas even at higher temperatures. For example, tenuous gas heated by a supernova explosion to $T = 10^8$ K may cool radiatively while it is exposed to the radiation field of the star association. To illustrate this, we assume a black body spectrum with a temperature $T_b = 3.5 \ 10^4 \,\mathrm{K}$, a total luminousity of $3 \ 10^5 \,\mathrm{L}_{\odot}$ geometrically diluted due to a distance of 1 pc and superimposed on the mean interstellar photon spectrum at the Sun's location (Black 1987). The resulting photon spectrum interacting with the cooling gas is displayed in Fig. 7, from which we derived a local acting energy flux of $10.1\,\mathrm{erg}\,\mathrm{s}^{-1}\,\mathrm{cm}^{-2}$ and a photoionization-rate of hydrogen of $4.0\,10^{-7}\,\mathrm{s}^{-1}$. The effective radiative cooling rate of the isochorically cooling gas $(N_{\rm H} = 1 \, {\rm cm}^{-3})$ is shown in Fig. 8 together with the heating rate. In this case the gas reaches an equilibrium temperature of T = 4024 K and remains in a middle ionized state (H II, He III, C III, C IV, N III, N IV, O III, O IV,..., Fe IV, Fe V). This thermal equilibrium is far from CIE, where gas at this temperature is known to be neutral.

The scenario we described above should not be confused with a typical H II region. Here we treat a thin gas, neglecting collisional deexcitation of forbidden lines and other important processes, e.g., line absorption. Nevertheless, we compare our result with that of the low density case in Osterbrock's textbook (1989). Apart from using different abundances, we calculate much higher ionization states than Osterbrock assumes. Thus the main coolants in our calculation are transitions from fine-structure levels of O III and O IV. The data for these infrared lines are taken from Jura & Dalgarno (1972). The resulting equilibrium temperature and ionization states also depend very sensitively on the shape of the ionizing photon spectrum. To test this, we calculated our model once more, but now neglecting the mean interstellar photon field. The slightly different photoionization and heating produces slightly lower ionization states accompanied with different, here somewhat less effective, line cooling. In this run the gas reaches thermal equilibrium at a temperature of T = 5167 K. From this example one also may get a rough idea about the sensitivity of such model calculations to the atomic data and physical processes taken into account.

However, such low equilibrium temperatures may well be established in low density H II regions: Celnik (1985) derived electron temperatures from radio continuum and recombination line observations of the Rosette nebula (NGC 2237–46) ranging from about 4000 K to 6000 K and a mean electron density of $11-16\,\mathrm{cm}^{-3}$. Even in the Galactic center, in the bar of Sagittarius A, the ratio of $\mathrm{Br}\alpha$ line emission to the radio continuum indicates electron temperatures ranging from 4000 K to 5000 K (Maloney et al. 1992).

Acknowledgements. T.S. would like to thank Prof. P.L. Biermann, for suggesting this fundamental area of astrophysics and many helpful discussions over years. Many problems have been clarified in numerous discussions with Drs. D. Breitschwerdt, K.-D. Fritz, D. Innes and Prof. H.J. Völk. We also thank Dr. R.J. Tuffs for a careful reading of the manuscript. Part of this work has been done in the framework of the Sonderforschungsbereich 328 (Entwicklung von Galaxien) of the Deutsche Forschungsgemeinschaft.

References

Aldrovandi S.M.V., Péquignot D., 1973, A&A 25, 137

Aldrovandi S.M.V., Péquignot D., 1976, A&A 47, 321

Allen C.W., 1973, Astrophysical Quantities, 3rd ed., Athlone Press,

Arnaud M., Rothenflug R., 1985, A&A Suppl. 60, 425

Biermann P., Kippenhahn R., Tscharnuter W., Yorke H., 1972, A&A

Binette L., Dopita M.A., Tuoly I.R., 1985, ApJ 297, 476

Black J.H., 1987, in: Interstellar Processes. Proceedings of the Symposium on Interstellar Processes, Grand Teton National Park 1986, eds. D.J. Hollenbach and H.A. Thronson, Jr., D. Reidel Publishing Company, Dordrecht, p. 731

Böhringer H., Hensler G., 1989, A&A 215, 147

Brinkmann W., Fink H.H., Smith A., Haberl F., 1989, A&A 221, 385

Byrne G.D., Hindmarsh A.C., 1987, J. Comput. Phys. 70, 1

Celnik W.E., 1985, A&A 144, 171

Cox D.P., 1972, ApJ 178, 143

Cox D.P., 1991, in: The interstellar disk-halo connection in galaxies. IAU Symposium No. 144, ed. H. Bloemen, Kluwer Academic Publishers, Dordrecht, p. 143

Cox D.P., Tucker W.H., 1969, ApJ 157, 1157

Dere K.P., Bartoe J.-D.F., Brueckner G.E., Dykton M.D., VanHoosier M.E., 1981, ApJ 249, 333

Gaetz T.J., Edgar R.J., Chevalier R.A., 1988, ApJ 329, 927

Gerola H., Kafatos M., McCray R., 1974, ApJ 189, 55

Halpern J.P., Grindlay J.E., 1980, ApJ 242, 1041

Hamilton A.J.S., Sarazin C.L., Chevalier R.A., 1983, ApJS 51, 115

Hamilton A.J.S., Sarazin C.L., Chevalier R.A., 1984, ApJ 284, 601

Hensler G., Burkert A., 1990, Ap&SS 170, 231

Innes D.E., 1985, PhD Thesis, University of London

Innes D.E., 1992, A&A 256, 660

Innes D.E., Giddings J.R., Falle S.A.E.G., 1987a, MNRAS, 224, 179

Innes D.E., Giddings J.R., Falle S.A.E.G., 1987b, MNRAS, 226, 67

Innes D.E., Giddings J.R., Falle S.A.E.G., 1987c, MNRAS, 227, 1021

Jura M., Dalgarno A., 1972, ApJ 174, 365

Kafatos M., 1973, ApJ 182, 433

Karzas W.J., Latter R., 1961, ApJS 6, 167

Kato T., 1976, ApJS 30, 397

Krolik J.H., McKee C.F., Tarter C.B., 1981, ApJ 249, 422

Landini M., Fossi B.C.M., 1971, Solar Physics 20, 322

Levich E.V., Sunyaev R.A., 1970, Astrophys. Letters 7, 69

Levich E.V., Sunyaev R.A., 1971, SvA 15, 363

Maloney P.R., Hollenbach D.J., Townes C.H., 1992, ApJ 401, 559

Morrison P., Sartori L., 1969, ApJ 158, 541

Novikov I.D., Thorne K.S., 1973, in: Black holes, Les Houches, eds. C. De Witt, B. De Witt, Gordon and Breach, New York

Osterbrock D.E., 1963, Planet. Space Sci. 11, 621

Osterbrock D.E., 1971, in: Nuclei of Galaxies, Pont. Acad. Scient. Scripta Varia 35, ed. D.J.K. O'Connell, Amsterdam

Osterbrock D.E., 1974, Astrophysics in gaseous nebulae, Freeman and Company, San Francisco

Osterbrock D.E., 1989, Astrophysics in gaseous nebulae and Active Galactic Nuclei, University Science Books, Mill Valley, p. 67

Osterbrock D.E., Wallace R.K., 1977, Astrophys. Letters 19, 11

Penston M.V., 1970, ApJ 162, 771

Reilman R.F., Manson S.T., 1978, Phys. Rev. A 18, 2124

Reilman R.F., Manson S.T., 1979, ApJS 40, 815

Savage B.D., 1991, in: The interstellar disk-halo connection in galaxies. IAU Symposium No. 144, ed. H. Bloemen, Kluwer Academic Publishers, Dordrecht, p. 131

Schaaf R., Pietsch W., Biermann P.L., Kronberg P.P., Schmutzler T., 1989, ApJ 336, 722

Schmutzler T., 1987, Thesis, University Bonn

Schmutzler T., 1993, A&A Suppl., in preparation

Schmutzler T., Lesch H., 1989, A&A 223, 71

Schmutzler T., Tscharnuter W.M., 1992, in: Physics of Active Galactic Nuclei. Proceedings of the Heidelberg Conference, 3-7 June 1991, eds. W. Duschl, S.J. Wagner, M. Camenzind, Springer, Berlin, p.

Shapiro P.R., Moore R.T., 1976, ApJ 207, 460

Shapiro P.R., Moore R.T., 1977, ApJ 217, 621

Shull J.M., 1979, ApJ 234, 761

Shull J.M., Van Steenberg M., 1982, ApJS 48, 95; erratum 1982, ApJS

Shull J.M., Woods D.T., 1985, ApJ 288, 50

Stern R., Wang E., Bowyer S., 1978, ApJS 37, 195

Tarter C.B., 1971, ApJ 168, 313

Vogel U., 1972, Ph. D. Thesis, University Bonn

Weisheit J.C., 1974, ApJ 190, 735

This article was processed by the author using Springer-Verlag TEX A&A macro package 1992.